


## Article

# One-Step Crystallization of Gahnite Glass-Ceramics in a Wide Thermal Gradient

Georgiy Yu. Shakhgildyan <sup>1,\*</sup> , Roman O. Alekseev <sup>1</sup>, Nikita V. Golubev <sup>1</sup>, Vitaliy I. Savinkov <sup>1</sup>, Andrey S. Naumov <sup>1</sup>, Natalia N. Presnyakova <sup>2</sup> and Vladimir N. Sigaev <sup>1</sup>

<sup>1</sup> Department of Glass and Glass-Ceramics, Mendeleev University of Chemical Technology of Russia, Moscow 125047, Russia

<sup>2</sup> National Research Center "Kurchatov Institute", Moscow 123098, Russia

\* Correspondence: georgiy.shakhgildyan@gmail.com

**Abstract:** The glass crystallization regime plays a crucial role in the fabrication of glass ceramics: it affects both phase composition and microstructure, and thus the properties of the final product. In the search for new glass-ceramic materials, the development of a proper heat-treatment schedule involves the utilization of numerous glass samples that need to be thermally treated and then investigated to determine the values of the target characteristics. In this study, we evaluated the effect of crystallization temperature on the glass structure, phase composition, and hardness of glass ceramics in the ZnO-MgO-Al<sub>2</sub>O<sub>3</sub>-SiO<sub>2</sub> system containing TiO<sub>2</sub> and ZrO<sub>2</sub> as nucleators. To maximize the number of heat treatments, we performed polythermal crystallization of the glass in a wide temperature range with the help of a gradient furnace. Using X-ray diffraction, Raman spectroscopy, and transmission electron microscopy, we showed the precipitation of gahnite nanocrystals as the main phase in the bulk of a single glass sample and observed a gradual change in its microstructure, transparency, and hardness. The dependence of Vickers hardness values on heat treatment temperature was found to follow a non-linear trend, revealing the optimal thermal range for glass crystallization.

**Keywords:** transparent glass-ceramics; crystallization; gradient furnace; polythermal crystallization; Vickers hardness; gahnite



**Citation:** Shakhgildyan, G.Y.; Alekseev, R.O.; Golubev, N.V.; Savinkov, V.I.; Naumov, A.S.; Presnyakova, N.N.; Sigaev, V.N. One-Step Crystallization of Gahnite Glass-Ceramics in a Wide Thermal Gradient. *ChemEngineering* **2023**, *7*, 37. <https://doi.org/10.3390/chemengineering7020037>

Academic Editors: Alirio E. Rodrigues and Andrew S. Paluch

Received: 8 March 2023

Revised: 10 April 2023

Accepted: 14 April 2023

Published: 18 April 2023



**Copyright:** © 2023 by the authors. Licensee MDPI, Basel, Switzerland. This article is an open access article distributed under the terms and conditions of the Creative Commons Attribution (CC BY) license (<https://creativecommons.org/licenses/by/4.0/>).

## 1. Introduction

The development of novel transparent glass ceramics is critical for a variety of applications in the modern world [1,2]. These materials combine the advantages of glassy and ceramic materials to provide unique sets of properties [3]. They are attractive for applications in the optical industry, engineering, and the field of photonics [4–6]. With their increased thermal and chemical stability and enhanced mechanical and optical properties, transparent glass ceramics can help improve the performance of products ranging from aerospace components to electronic devices [4]. It is important to determine an optimal heat-treatment schedule, in particular the crystallization temperature of a glass, as it will determine the properties and usefulness of glass ceramics. By understanding the crystallization process, the properties of the material can be tailored for specific applications, and the performance of the material can be optimized [7].

Basic information about the crystallization temperatures of glass is typically used for the development of the crystallization regime to obtain glass-ceramic materials with the desired properties [8]. There are typically two steps in such regimes: crystal nucleation occurs in the first step, and crystal growth takes place in the second step [9]. The appearance of numerous exothermic peaks in a DSC curve usually suggests that several phases precipitate during non-isothermal heating. According to the structure, size, and quantity of crystals, each crystal phase can have profound effects on glass-ceramic properties, such as increased hardness or fracture toughness. Recent studies show that among the wide variety of transparent glass ceramics, gahnite-based materials could provide the best combinations

of mechanical and optical properties. Kurajica S. et al. reported a systematic study of the crystallization of glasses in the  $\text{ZnO-Al}_2\text{O}_3\text{-SiO}_2$  system nucleated with  $\text{TiO}_2$ , showing possibilities for gahnite precipitation in different glass compositions [10], while Mitchell A. L. et al. provided a detailed microstructural analysis of gahnite glass-ceramics and showed that  $\text{ZnAl}_2\text{O}_4$  crystallites were found in proximal locations to  $\text{ZrO}_2$  and not in a core-shell arrangement [11]. Molla A.R. obtained transparent gahnite glass ceramics with a homogeneous distribution of nanocrystals; up to a 30% increase in Vickers hardness compared to that of the parent glass was reported [12]. The ability to obtain transparent gahnite glass ceramics suitable for ion exchange was reported by Wang S. et al. The Vickers hardness of the glass ceramics increased from approximately 6 to 7 GPa after the ion exchange process [13]. Loiko P. et al. reported on the synthesis of  $\text{Co}^{3+}$ -doped gahnite glass ceramics with thermal and optical properties suitable for extended-cavity Er lasers [14].

However, transparent glass ceramics have limits on the size and number of crystals that can be formed to retain the transparency of the composite material [3]. It is the case that transparent glass ceramics are produced by treatments at relatively low temperatures for long holding times to precipitate small crystals. In the search for new transparent glass-ceramic materials, the development of a proper crystallization regime involves numerous glass samples that need to be thermally treated and then studied to determine the values of the target properties. The determination of the time-temperature conditions in the first step of the two-step regime is especially complicated.

During polythermal crystallization, on the other hand, crystallization of glass occurs over a broader temperature range, requiring only a single glass sample. Initially, such a technique was used in the production of optical electro-vacuum and other industrial glasses for the study of 'glass crystallizability', that is, the determination of the upper and lower crystallization temperatures during visual inspection of the crystallized glass sample [15]. This method is still common for the study of glass structure and properties in the thermal gradient [16,17]. Moreover, the crystallization of glass in the thermal gradient could be a powerful tool not only for the quick determination of crystallization parameters but also for the production of novel materials. Different types of gradient crystallization were applied to the glasses. Gardopee G. J. et al. demonstrated [18] the formation of highly oriented layers of lithium disilicate crystals on the surface of a glass placed on a hot stage and treated under the thermal gradient. Ochi Y. et al. showed [19] oriented crystallization of fresnoite polar glass ceramics. Sigaev V.N. et al. produced ferroelectric phases of the stillwellite family with excellent pyroelectric properties in glasses during the crystallization in the thermal gradient [20]. The so-called 'up-gradient crystallization' process, which is the crystallization of an amorphous sample upon its moving through a thermal gradient, was reviewed by Kim S. J. et al. [21], showing that highly oriented microstructures may be produced in glass. Moreover, ultrafast laser irradiation (i.e., direct laser writing) could also be described in terms of gradient crystallization of glass since local nonlinear absorption of the laser beam induces a high thermal gradient and heat transfer, which play the main role in local glass crystallization [22,23].

Thus, the polythermal crystallization technique allows the dependence of structure and properties on heat treatment conditions over a wide temperature range and therefore helps optimize the fabrication of glass ceramics. In the present study, we used polythermal crystallization and a set of instrumental analysis methods to evaluate the effect of crystallization temperature on the glass structure as well as on the microstructure and hardness of the glass-ceramics in the  $\text{ZnO-MgO-Al}_2\text{O}_3\text{-SiO}_2$  system.

## 2. Materials and Methods

### 2.1. Glass Production and Polythermal Crystallization

We produced the glass with the following nominal molar compositions: 1.1  $\text{Na}_2\text{O}$ ; 0.3  $\text{As}_2\text{O}_3$ ; 5.9  $\text{TiO}_2$ ; 1.2  $\text{ZrO}_2$ ; 20.1  $\text{ZnO}$ ; 13.6  $\text{MgO}$ ; 9.8  $\text{Al}_2\text{O}_3$ ; and 48.0  $\text{SiO}_2$ . A similar composition was previously used in our work to study the properties of transparent glass ceramics with high hardness [24]. The addition of  $\text{Na}_2\text{O}$  was used as a flux,  $\text{As}_2\text{O}_3$  as a

fining agent for the glass melt, and  $\text{TiO}_2$  and  $\text{ZrO}_2$  as nucleators. High-purity raw materials (reagent grade) were weighed, mixed, and used for the preparation of the batch, which was calculated to produce 500 g of glass. The batch was loaded into the corundum crucible and placed in the chamber of the bottom-loading electrical furnace equipped with  $\text{MoSi}_2$  heating elements (Promtermo Ltd., Moscow, Russia). The furnace was heated up to  $1620^\circ\text{C}$  and kept at this temperature for 2 h to homogenize and refine the glass melt. After that, the melt was poured into the preheated mold, which was subsequently transferred into a muffle furnace (Termokeramika Ltd., Moscow, Russia) for annealing of the casting at  $550^\circ\text{C}$  for 4 h. The fabricated glass was visually transparent, free of bubbles, and represented a block of size  $\sim 150 \times 90$  mm (Figure S1 in the Supplementary).

The block was cut along the long side, and the glass sample of 120 mm in length and 10 mm in width was obtained and optically polished. A homemade gradient electrical furnace—consisting of a 200-mm horizontally mounted ceramic tube, on whose outer surface a FeCrAl wire was wound with a variable pitch—was used for the polythermal crystallization of the glass. The temperature distribution inside the furnace was measured directly by a portable thermocouple with a 10 mm step. The glass sample was placed inside the furnace and kept in the  $550$ – $900^\circ\text{C}$  temperature range for 1 h. After that, the sample was rapidly pulled out of the furnace, examined, and cut for further study.

## 2.2. Glass and Glass-Ceramics Characterization

The digital photos of the glass block and the sample were taken with the built-in camera (iPhone 11). The refractive index of the glass was measured with an Abbe refractometer, the DR-M4 (ATAGO Co., Ltd., Tokyo, Japan), at  $589$  nm at  $25^\circ\text{C}$ . Non-isothermal crystallization and length changes on heating of the bulk glass were investigated by the simultaneous thermal analyzer STA 449 F3 Jupiter (NETZSCH, Waldkraiburg, Germany) with a dynamic flow atmosphere of Ar and the dilatometer DIL 402 PC (NETZSCH, Germany), respectively. NTEGRA Spectra Spectrometer (NT-MDT Co., Zelenograd, Moscow, Russia) with the Ar laser beam ( $488$  nm excitation wavelength) was used to record Raman spectra from the different zones of the thermally treated glass sample. An X-ray diffraction (XRD) analysis of the initial and heat-treated glasses was carried out on a diffractometer (D2 Phaser; Bruker, Mannheim, Germany) employing nickel-filtered  $\text{CuK}\alpha$  radiation. Prior to the analysis, the heat-treated glass sample was cut into slices in four zones (designated as A–D), and then each slice as well as the initial glass was ground. Crystalline phases were identified by comparing the peak positions and relative intensities in XRD patterns with the ICDD PDF-2 database (released in 2011). The same powdered samples were used to study their microstructure by high-resolution transmission electron microscopy (HRTEM) with the help of a transmission electron microscope, the Titan 80-300 S/TEM (Thermo Fisher Scientific FEI, Waltham, MA, USA), equipped with a spherical aberration corrector and combined with the energy-dispersive X-ray spectrometer (EDXS). HRTEM images were obtained in  $300$  kV mode. The HRTEM images were processed with the ImageJ software [25]. Vickers hardness was determined along the thermally treated glass sample using the HVS-1000 hardness tester (Zhengyi Testing Machinery, Yangzhou, China) at a load of  $200$  g for  $10$  s. Ten indentations were performed under identical loading conditions to calculate the mean for each sample.

## 3. Results and Discussion

### 3.1. Polythermal Crystallization of Glass

Figure 1 shows the differential scanning calorimetry (DSC) thermogram and thermal expansion curve for the initial glass. One can see from the DSC curve that the glass transition temperature ( $T_g$ ) is  $685^\circ\text{C}$ , which is somewhat lower than  $T_g$  for similar glasses [26], probably due to the considerably different content of  $\text{ZnO}$  and  $\text{Al}_2\text{O}_3$  in our glass. Sharp peaks in the DSC trace imply bulk crystallization, and they are consistent with the visual inspection of the sample after treatment in the gradient furnace. These exothermic peaks observed at temperatures ( $T_c$ )  $816$ ,  $872$ , and  $928^\circ\text{C}$  indicate complex crystallization of the

glass with the precipitation of several crystalline phases. The dilatometric softening point ( $T_S$ ) was estimated to be  $746^\circ\text{C}$ , and the coefficient of thermal expansion in the  $50\text{--}500^\circ\text{C}$  range was calculated to be  $5.6 \times 10^{-6}^\circ\text{C}^{-1}$  (Figure 2b). The origin of the plateau detected just below  $\sim 700^\circ\text{C}$  in the thermal expansion curve is likely connected with the beginning of crystallization, as will be suggested below by XRD data. Table 1 summarizes all the studied properties of the synthesized glass.

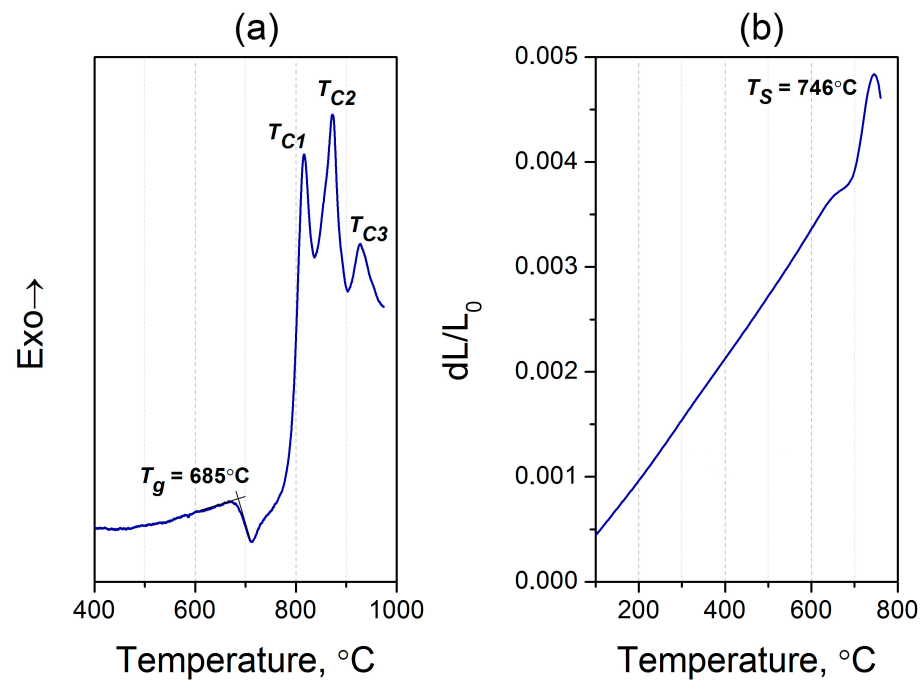


Figure 1. (a) The DSC curve, and (b) the dilatometric curve of the initial glass.

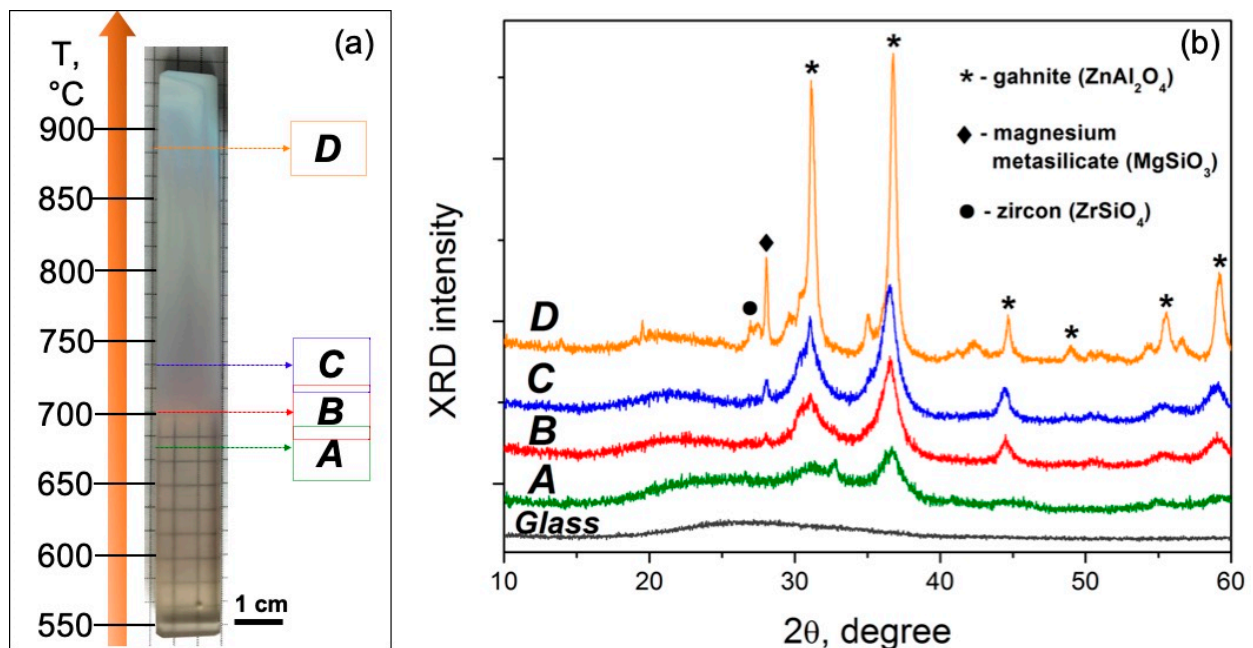


Figure 2. (a) Image of the glass sample after the polythermal crystallization. Designations A–D indicated in the figure denote the zones of further analysis. (b) XRD patterns recorded from the corresponding zones A–D of the treated sample and initial glass.

**Table 1.** Measured properties of the synthesized glass.

Density, g/cm <sup>3</sup>	T <sub>g</sub> , °C	T <sub>C1</sub> , °C	T <sub>C2</sub> , °C	T <sub>C3</sub> , °C	T <sub>S</sub> , °C	CTE <sub>50–500 °C</sub> , °C <sup>−1</sup>	Refractive Index
3.5	685	816	872	928	746	5.6 × 10 <sup>−6</sup>	1.56

Figure 2a shows the image of the glass sample after crystallization in the 550–900 °C range for 1 h. One can clearly see that up to 700 °C (zone A), the glass is visually transparent. In the 700–725 °C range (zone B), the glass becomes translucent due to the intensification of the phase separation process. As the temperature rises above 725 °C (zones C and D), the sample becomes opaque to visible light.

The XRD patterns of the initial glass as well as of the powdered samples obtained from zones A–D are presented in Figure 2b. No diffraction peaks are observed in the XRD pattern of the initial glass, confirming its amorphous nature. For the heat-treated samples, the main crystalline phase is identified as gahnite (ZnAl<sub>2</sub>O<sub>4</sub>, PDF #01-071-0968). Diffraction peaks of this phase, with the strongest reflection observed at around 2θ = 37°, could be found in all patterns. When temperature increases, the position of the amorphous halo shifts to lower 2θ values, suggesting a compositional change in the residual glass caused by crystallization. Along with this change, the intensity of the peaks corresponding to gahnite increases while their width reduces, indicating the growth of the crystals. Additionally, a peak at around 2θ = 28° appears and becomes larger in the XRD patterns of zones from B to D. Most probably, it is attributed to magnesium metasilicate (MgSiO<sub>3</sub>, PDF #01-074-0816). Moreover, a weak reflection of zircon (ZrSiO<sub>4</sub>, PDF #01-071-0991) is seen in the XRD pattern recorded from zone D (a peak at around 2θ = 27°). Besides these compounds, some weak reflections of other phases are also detected, which can probably be assigned to zinc titanate (ZnTiO<sub>3</sub>, PDF #01-085-0547), rutile (TiO<sub>2</sub>, PDF #01-070-7347), and srilankite (ZrTiO<sub>4</sub>, PDF #00-034-0415).

To estimate how the crystal size of the main phase (gahnite) changes with temperature along the sample, we used the well-known Scherrer's equation:

$$D = \frac{K\lambda}{\Delta \cos \theta}, \quad (1)$$

where λ is the wavelength of the X-ray radiation, θ is the diffraction angle, Δ is the width of the peak at half of its maximum, and K is the constant (used as K = 1) [27]. Analysis of the broadening of the XRD peak at about 37° revealed the growth of the gahnite crystals from ~5 to 20 nm. Table 2 summarizes crystallite sizes estimated from the XRD patterns.

**Table 2.** Sizes of gahnite crystals are calculated by Scherrer's equation.

Zone	Crystallite Size, nm
A	5.4
B	7.7
C	9.0
D	18.5

One can see that crystallization of the glass starts at temperatures just above T<sub>g</sub> (Figure 2, zone A), supporting the interpretation of dilatometry data (Figure 1b). As a result, the size and content of precipitated crystals are small enough (~5 nm) to avoid intense light scattering. Crystal formation at such low temperatures also suggests that there is considerable chemical differentiation in the glass, with the formation of regions similar to gahnite in composition and structure.

### 3.2. Transformation of Glass Structure and Properties in the Thermal Gradient

Figure 3 presents Raman spectra recorded from different zones, as depicted in Figure 2a. The spectrum of the initial glass as well as the spectrum of the glass from zone A is charac-



terized by two broad bands located at  $\sim 790$  and  $\sim 900\text{ cm}^{-1}$ . One can see a slight change in the intensity ratio between the  $\sim 790$  and  $\sim 900\text{ cm}^{-1}$  bands in the spectrum from zone A compared to that of the glass. According to the previous studies [28,29], this implies that a phase separation process takes place: the  $\sim 900\text{ cm}^{-1}$  band is assigned to  $[\text{TiO}_4]$ -tetrahedrons built into the glass matrix, while the band at  $\sim 790\text{ cm}^{-1}$  is likely to correspond to the vibrations of Ti–O bonds in the amorphous zinc aluminotitanate phase. The observed evolution of the intensity ratio with thermal treatment is evidence of the progress of the phase separation process.

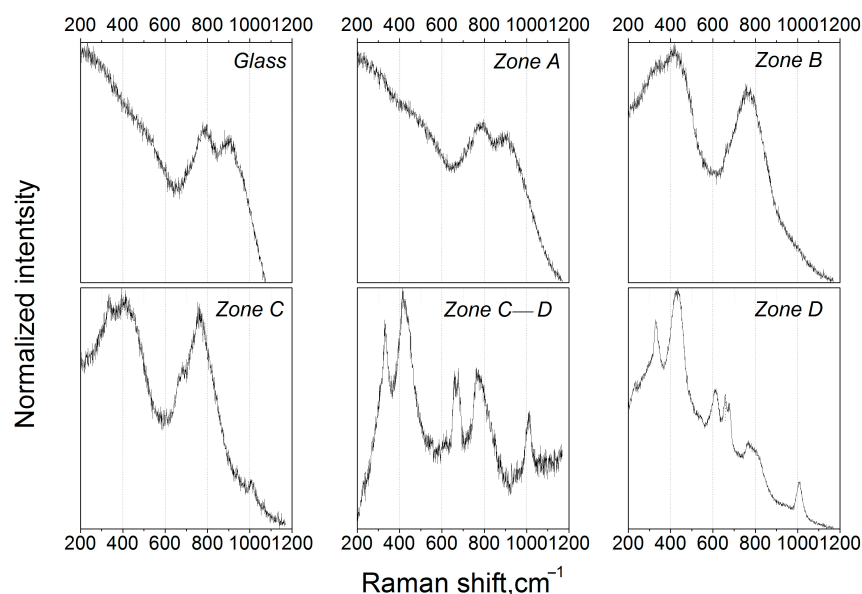


**Figure 3.** Raman spectra recorded from different zones of the glass sample (symbols A–D correspond to Figure 2a).

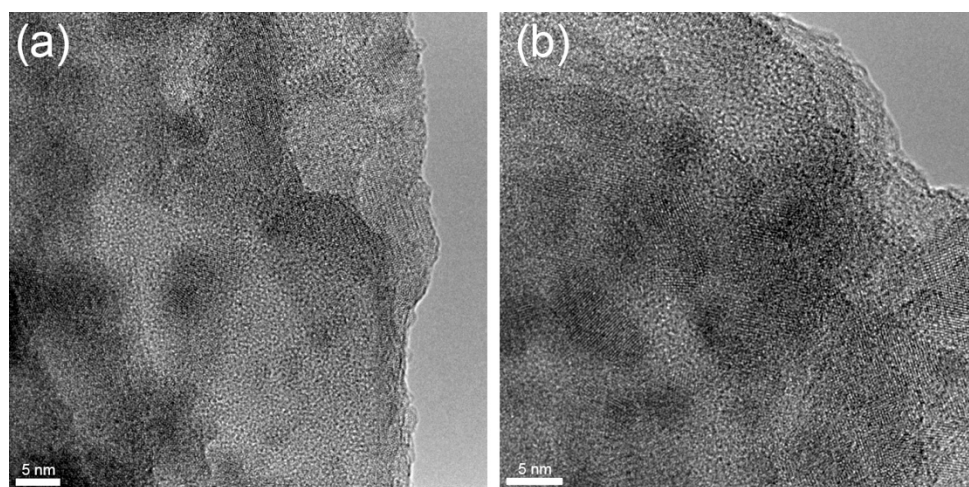
The spectrum from zone B reflects changes in the glass structure that we previously highlighted by XRD and a visual inspection: first of all, the band at  $\sim 416\text{ cm}^{-1}$  appeared, indicating the precipitation of gahnite crystals; this band corresponds to one of the most intensive lines of the model polycrystalline  $\text{ZnAl}_2\text{O}_4$  located at  $417\text{ cm}^{-1}$  [28]. This band also has a shoulder at  $330\text{ cm}^{-1}$ , which can be assigned to the weakly resolved band of magnesium metasilicate [30]. The bands at  $\sim 790$  and  $900\text{ cm}^{-1}$  disappeared, indicating the end of the liquid-liquid phase separation, while a new band at  $\sim 770\text{ cm}^{-1}$  appeared, which could be assigned to Al–O symmetric stretching vibrations of  $[\text{AlO}]_x$  segments in  $\text{ZnAl}_2\text{O}_4$  crystals [31,32]. These results are in line with the XRD data, confirming the precipitation of the gahnite crystals and the early stages of the magnesium metasilicate formation in zone B.

Further transformation of glass structure in the thermal gradient is depicted on the spectrum from zone C. The shoulder at  $\sim 330\text{ cm}^{-1}$  turned toward the distinguishable band, while the band at  $\sim 416\text{ cm}^{-1}$  retained its shape and spectral position. One can also observe a weakly resolved band at  $\sim 1008\text{ cm}^{-1}$ , which is fully resolved in the following spectra. This band corresponds to the antisymmetric  $\nu_3[\text{SiO}_4]$  stretching vibrations of  $\text{ZrSiO}_4$  (zircon) [33]. In the spectrum of zone D, bands at  $\sim 330\text{ cm}^{-1}$ ,  $\sim 677\text{ cm}^{-1}$ , and  $763\text{ cm}^{-1}$  correspond to magnesium metasilicate [30], a band at  $\sim 1008\text{ cm}^{-1}$  to zircon, and other observed bands to gahnite.

These preliminary results indicate that the single glass sample studied undergoes crucial structural changes during the treatment in the thermal gradient. Hence, the method of polythermal crystallization paves the way for a quick overview study of different glass and glass-ceramic samples.

In order to further investigate the internal structure of the studied glass treated with a thermal gradient, we used the HRTEM method in all zones from A to D. Figure 4 shows

HRTEM images from zone A. Images contain nanoscale areas (up to 5–7 nm) with a perceptible chemical contrast; moreover, in some areas, one can observe crystal planes that correspond to the formation of nanocrystals. It is known [34] that during the nucleation process in glasses, different types of nuclei could be formed that are essential for further crystallization of the main phase. Due to their small size, it is impossible to detect them by XRD or Raman spectroscopy. Hence, the performed HRTEM analysis of zone A does not provide a clear conclusion about the type of precipitated crystals, i.e., whether it is the gahnite phase or other phases, but based on the XRD data (Figure 2b), we can assume that most of the observed areas with crystal planes correspond to gahnite. Moreover, the mean measured the size of the observed crystals is  $5.2 \pm 0.7$  nm, which is perfectly in line with the size estimated by XRD (Table 1).



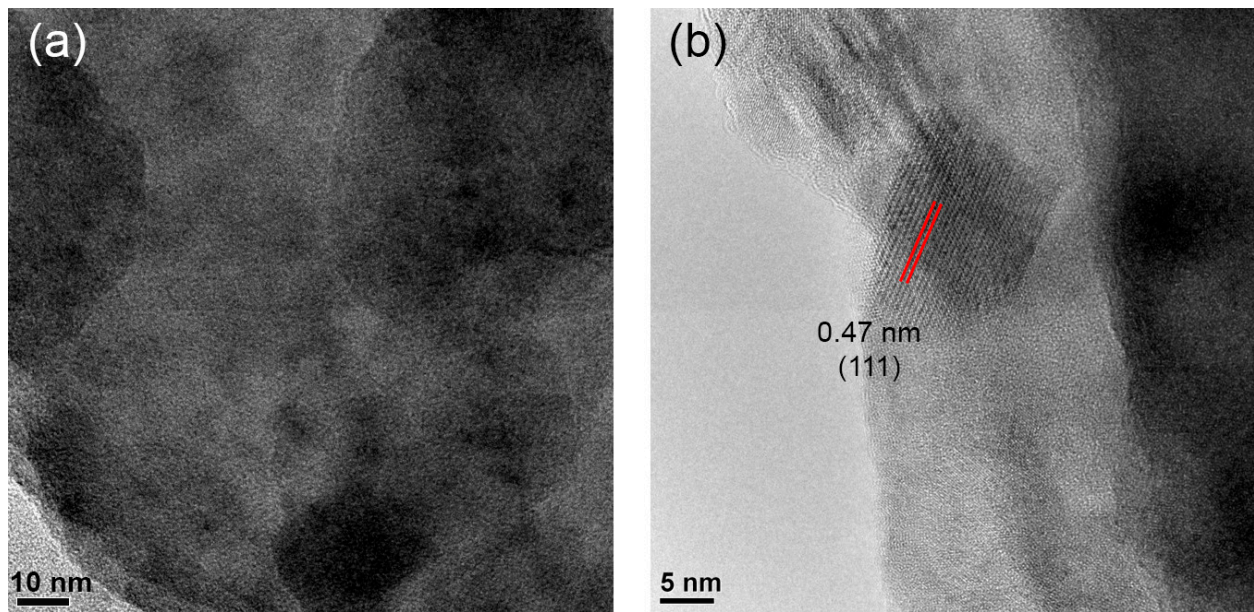
**Figure 4.** (a,b) HRTEM images of zone A in different areas.

Figure 5 presents HRTEM images of zone B. One can see crystals with sizes up to 10–13 nm. The interplanar distance of the well-resolved single crystal was measured to be 0.47 nm (Figure 5a), which corresponds to the gahnite (111) crystallographic plane spacing (PDF #01-071-0968). These findings further confirm gahnite crystallization in zone B of the single glass samples during the polythermal crystallization in the thermal gradient.

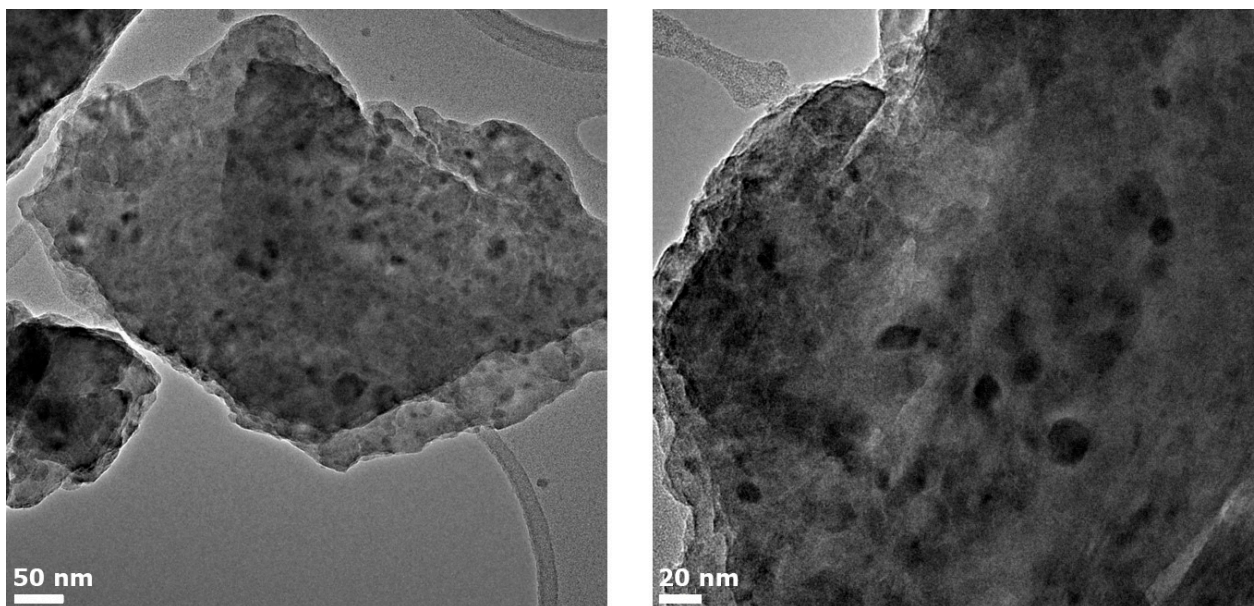
An overview of the glass microstructure in zone C is presented in Figure 6. Crystals with sizes up to 40 nm can be found. According to the XRD data, two types of crystals (gahnite and magnesium metasilicate) are expected to be present. The X-ray peak broadening analysis using a peak at around  $2\theta = 28^\circ$  assigned preliminary to magnesium metasilicate showed that the crystal size of this phase is about 29.8 nm, while the size of gahnite crystals is equal to  $\sim 9.0$  nm (Table 1). A similar significant difference in sizes could be observed in the provided TEM images: there are two groups of crystals with mean sizes of  $11.2 \pm 1.3$  nm and  $32 \pm 1.8$  nm, respectively, corresponding to the presence of two crystal phases.

Figure 7 presents captured TEM images from zone D. Single gahnite crystals of 22.1 nm and 19.8 nm diameter showcasing a well-resolved 0.47 nm and 0.29 nm interplanar spacing corresponded to (111) and (220) crystallographic planes and could be observed in Figure 7b,c. These results match perfectly with the calculated sizes from the XRD data. Despite not being able to capture magnesium metasilicate and zircon crystals with well-resolved interplanar spacing, according to XRD data, zone D contains magnesium metasilicate and zircon crystals as well.





**Figure 5.** (a,b) HRTEM images of zone B in different areas. Red lines highlight the interplanar distance.



**Figure 6.** TEM images of zone C.

To finally demonstrate the usefulness of the polythermal crystallization method for optimizing heat treatment conditions, we studied the evolution of Vickers hardness values along the glass sample treated in a wide temperature range. Figure 8 shows the results of the Vickers hardness measurements, which demonstrated a nonlinear change. In zone A, hardness values began to increase with respect to the cold end of the glass sample due to the precipitation of gahnite crystals. Further increases in temperature in zones B and C resulted in higher Vickers hardness values, reaching more than 10 GPa. The ends of zone C and zone D were characterized by a distinct decrease in hardness, down to 8 GPa. The observed decline of hardness values in the high-temperature zones of the glass sample could be attributed to the negative effects of multi-phase precipitation and rapid crystal growth. In fact, the remarkable mechanical properties of glass-ceramics compared to the initial glass are not only due to crystal phase precipitation but also to low-stress values at glass-crystal interfaces [35]. The rapid growth rate of different crystals with relatively large



sizes in zones C and D at high treatment temperatures caused a decrease in the hardness of glass ceramics. The obtained Vickers hardness values are consistent with the recent findings for transparent glass ceramics in similar glass-forming systems, where values up to 10 GPa can be potentially achieved [36,37].

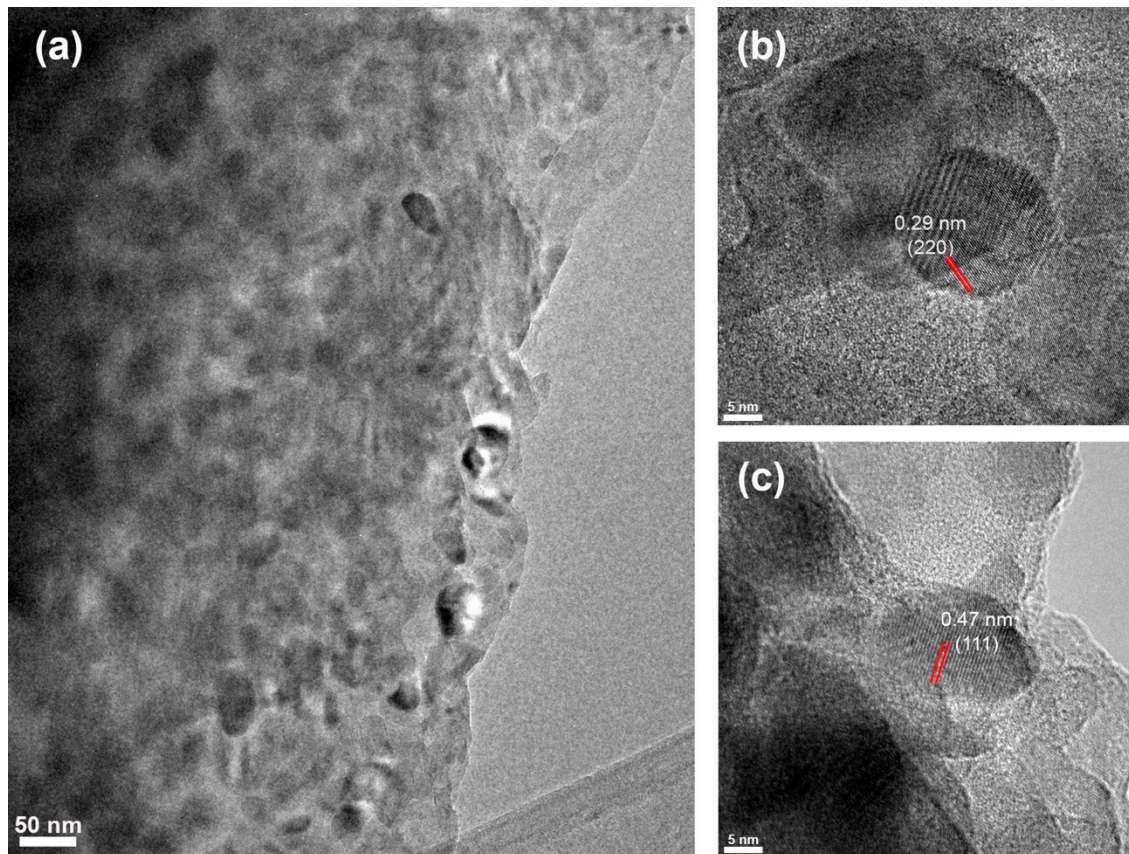


**Figure 7.** (a) TEM images of zone D; (b,c) HRTEM images of gahnite nanocrystals with the corresponding interplanar spacings. Red lines highlight the interplanar distance.

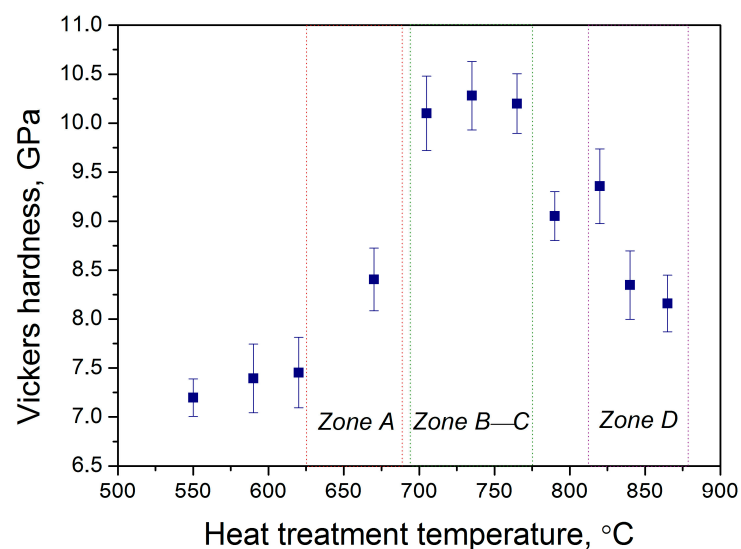


**Figure 8.** Vickers hardness values along the glass sample after the polythermal crystallization.

Still, the achieved results for zones A and B, where transparent/translucent glass ceramics with high hardness could be obtained, obviously make the studied composition

of glass attractive for further research. In general, polythermal crystallization has proved to be a versatile method for the research and development of glass ceramics. The utilization of a thermal gradient enabled the monitoring of crystal growth in the single glass sample and controlled its microstructure. Thus, polythermal crystallization is an efficient method for the evaluation of glass crystallization and the production of glass ceramics with superior mechanical properties.

#### 4. Conclusions

To conclude, employing the polythermal crystallization method, we managed to reveal heat-treatment conditions that provided the required combination of target properties (transparency and high hardness) for the glass-ceramics in the ZnO-MgO-Al<sub>2</sub>O<sub>3</sub>-SiO<sub>2</sub> system. Using a single glass sample of 120 mm in length, we investigated the transformation of glass structure and properties over a wide temperature range. Based on the XRD, HRTEM, and Raman spectroscopy results, we showed that transparent glass ceramics with gahnite as the main crystal phase were obtained below 725 °C after 1 h of heat treatment. Further, an increase in temperature led to the growth of gahnite crystals up to ~20 nm as well as the precipitation of other phases and loss of transparency. It was found that the Vickers hardness values of fabricated glass ceramics can reach 10–10.5 GPa. The high hardness achieved for the transparent/translucent parts of the glass-ceramic sample (zones A and B) makes this composition an attractive option for further research. The structural analysis of the studied material is essential to understanding the physics and chemistry that govern the evolution of its microstructure and phase composition. This knowledge can be used in the future to optimize the production process of the glass-ceramics, as well as their properties, for a range of applications in electronic devices and photonics.

**Supplementary Materials:** The following supporting information can be downloaded at: <https://www.mdpi.com/article/10.3390/chemengineering7020037/s1>, Figure S1: Photo of the glass block. The text is given for the visualization of the transparency of glass block and means the following: “MUCTR. Mendeleev University of Chemical Technology of Russia”.

**Author Contributions:** Conceptualization, G.Y.S. and V.N.S.; validation, G.Y.S. and V.I.S.; investigation, N.V.G., R.O.A., A.S.N. and N.N.P.; writing—original draft preparation, G.Y.S.; visualization, G.Y.S.; supervision, V.N.S.; funding acquisition, G.Y.S. All authors have read and agreed to the published version of the manuscript.

**Funding:** This research was funded by the Russian Science Foundation under grant no. 22-73-00236.

**Data Availability Statement:** The data presented in this study are available on request from the corresponding author.

**Conflicts of Interest:** The authors declare no conflict of interest.

#### References

1. Liu, X.; Zhou, J.; Zhou, S.; Yue, Y.; Qiu, J. Transparent Glass-Ceramics Functionalized by Dispersed Crystals. *Prog. Mater. Sci.* **2018**, *97*, 38–96. [CrossRef]
2. Shakhgildyan, G.; Lipatiev, A.; Lotarev, S.; Fedotov, S.; Sigaev, V. Glass: Home of the Periodic Table. *Front. Chem.* **2020**, *8*, 384. [CrossRef]
3. Alekseeva, I.; Dymshits, O.; Tsenter, M.; Zhilin, A.; Golubkov, V.; Denisov, I.; Skoptsov, N.; Malyarevich, A.; Yumashev, K. Optical Applications of Glass-Ceramics. *J. Non-Cryst. Solids* **2010**, *356*, 3042–3058. [CrossRef]
4. Sakamoto, A.; Yamamoto, S. Glass-Ceramics: Engineering Principles and Applications. *Int. J. Appl. Glass Sci.* **2010**, *1*, 237–247. [CrossRef]
5. Gallo, L.S.; Villas Boas, M.O.C.; Rodrigues, A.C.M.; Melo, F.C.L.; Zanutto, E.D. Transparent Glass-Ceramics for Ballistic Protection: Materials and Challenges. *J. Mater. Res. Technol.* **2019**, *8*, 3357–3372. [CrossRef]
6. Shakhgildyan, G.; Durymanov, V.; Ziyatdinova, M.; Atroshchenko, G.; Golubev, N.; Trifonov, A.; Chereuta, O.; Avakyan, L.; Bugaev, L.; Sigaev, V. Effect of Gold Nanoparticles on the Crystallization and Optical Properties of Glass in ZnO-MgO-Al<sub>2</sub>O<sub>3</sub>-SiO<sub>2</sub> System. *Crystals* **2022**, *12*, 287. [CrossRef]
7. Beall, G.H.; Pinckney, L.R. Nanophase Glass-Ceramics. *J. Am. Ceram. Soc.* **2004**, *82*, 5–16. [CrossRef]
8. Komatsu, T. Design and Control of Crystallization in Oxide Glasses. *J. Non-Cryst. Solids* **2015**, *428*, 156–175. [CrossRef]

9. Deubener, J.; Allix, M.; Davis, M.J.; Duran, A.; Höche, T.; Honma, T.; Komatsu, T.; Krüger, S.; Mitra, I.; Müller, R.; et al. Updated Definition of Glass-Ceramics. *J. Non-Cryst. Solids* **2018**, *501*, 3–10. [\[CrossRef\]](#)
10. Kurajica, S.; Šipušić, J.; Zupancic, M.; Brautović, I.; Albrecht, M. ZnO-Al<sub>2</sub>O<sub>3</sub>-SiO<sub>2</sub> Glass Ceramics: Influence of Composition on Crystal Phases, Crystallite Size and Appearance. *J. Non-Cryst. Solids* **2021**, *553*, 120481. [\[CrossRef\]](#)
11. Mitchell, A.L.; Perea, D.E.; Wirth, M.G.; Ryan, J.V.; Youngman, R.E.; Rezikyan, A.; Fahey, A.J.; Schreiber, D.K. Nanoscale Microstructure and Chemistry of Transparent Gahnite Glass-Ceramics Revealed by Atom Probe Tomography. *Scr. Mater.* **2021**, *203*, 114110. [\[CrossRef\]](#)
12. Molla, A.R.; Rodrigues, A.M.; Singh, S.P.; Lancelotti, R.F.; Zanutto, E.D.; Rodrigues, A.C.M.; Reza Dousti, M.; de Camargo, A.S.S.; Magon, C.J.; Silva, I.D.A. Crystallization, Mechanical, and Optical Properties of Transparent, Nanocrystalline Gahnite Glass-Ceramics. *J. Am. Ceram. Soc.* **2017**, *100*, 1963–1975. [\[CrossRef\]](#)
13. Wang, S.; Guo, Y.; Lu, Y.; Liu, C.; Deng, Z.; Han, N.; Cui, J. Microstructure and Ion-Exchange Properties of Transparent Glass-Ceramics Containing Zn<sub>2</sub>TiO<sub>4</sub>/α-Zn<sub>2</sub>SiO<sub>4</sub> Nanocrystals. *J. Eur. Ceram. Soc.* **2022**, *42*, 3595–3602. [\[CrossRef\]](#)
14. Loiko, P.; Belyaev, A.; Dymshits, O.; Evdokimov, I.; Vitkin, V.; Volkova, K.; Tsenter, M.; Volokitina, A.; Baranov, M.; Vilejshikova, E.; et al. Synthesis, Characterization and Absorption Saturation of Co:ZnAl<sub>2</sub>O<sub>4</sub> (Gahnite) Transparent Ceramic and Glass-Ceramics: A Comparative Study. *J. Alloys Compd.* **2017**, *725*, 998–1005. [\[CrossRef\]](#)
15. Ignat'ev, A.I.; Shalamaiko, E.E.; Shmatok, L.K. Crystallizability of Optical Glasses and Their Melts. *Glass Ceram.* **1995**, *52*, 84–86. [\[CrossRef\]](#)
16. Alekseev, R.O.; Romanov, N.A.; Savinkov, V.I.; Klimenko, N.N.; Sigaev, V.N. Multicomponent Optical Glasses with High Refractive Index. *Glass Ceram.* **2021**, *78*, 3–7. [\[CrossRef\]](#)
17. Velmuzhov, A.P.; Sukhanov, M.V.; Plekhovich, A.D.; Suchkov, A.I.; Shiryayev, V.S.; Churbanov, M.F. Preparation and Investigation of Glasses in the GeS<sub>2</sub>-GeI<sub>4</sub> System. *Opt. Mater.* **2015**, *42*, 340–344. [\[CrossRef\]](#)
18. Gardopee, G.J.; Newnham, R.E.; Halliyal, A.G.; Bhalla, A.S. Pyroelectric Glass-ceramics. *Appl. Phys. Lett.* **1980**, *36*, 817–818. [\[CrossRef\]](#)
19. Ochi, Y.; Meguro, T.; Kakegawa, K. Orientated Crystallization of Fresnoite Glass-Ceramics by Using a Thermal Gradient. *J. Eur. Ceram. Soc.* **2006**, *26*, 627–630. [\[CrossRef\]](#)
20. Sigaev, V.N.; Sarkisov, P.D.; Stefanovich, S.Y.; Pernice, P.; Aronne, A. Glass Ceramic Textures Based on New Ferroelectric Complex Oxides. *Ferroelectrics* **1999**, *233*, 165–185. [\[CrossRef\]](#)
21. Kim, S.J.; Birnie, D.P.; Zelinski, B.J.J.; Uhlmann, D.R. Practical Limits on Up-Gradient Crystallization. *J. Non-Cryst. Solids* **1995**, *181*, 291–300. [\[CrossRef\]](#)
22. Lipatiev, A.S.; Lipateva, T.O.; Lotarev, S.V.; Okhrimchuk, A.G.; Larkin, A.S.; Presnyakov, M.Y.; Sigaev, V.N. Direct Laser Writing of LaBGeO<sub>5</sub> Crystal-in-Glass Waveguide Enabling Frequency Conversion. *Cryst. Growth Des.* **2017**, *17*, 4670–4675. [\[CrossRef\]](#)
23. Shakhgildyan, G.Y.; Lipatiev, A.S.; Fedotov, S.S.; Vetchinnikov, M.P.; Lotarev, S.V.; Sigaev, V.N. Microstructure and Optical Properties of Tracks with Precipitated Silver Nanoparticles and Clusters Inscribed by the Laser Irradiation in Phosphate Glass. *Ceram. Int.* **2021**, *47*, 14320–14329. [\[CrossRef\]](#)
24. Shakhgil'dyan, G.Y.; Savinkov, V.I.; Shakhgil'dyan, A.Y.; Alekseev, R.O.; Naumov, A.S.; Lopatkina, E.V.; Sigaev, V.N. Effect of Sitalization Conditions on the Hardness of Transparent Sitalis in the System ZnO-MgO-Al<sub>2</sub>O<sub>3</sub>-SiO<sub>2</sub>. *Glass Ceram.* **2021**, *77*, 426–428. [\[CrossRef\]](#)
25. Schneider, C.A.; Rasband, W.S.; Eliceiri, K.W. NIH Image to ImageJ: 25 Years of Image Analysis. *Nat. Methods* **2012**, *9*, 671–675. [\[CrossRef\]](#) [\[PubMed\]](#)
26. Hunger, A.; Carl, G.; Rüssel, C. Formation of Nano-Crystalline Quartz Crystals from ZnO/MgO/Al<sub>2</sub>O<sub>3</sub>/TiO<sub>2</sub>/ZrO<sub>2</sub>/SiO<sub>2</sub> Glasses. *Solid State Sci.* **2010**, *12*, 1570–1574. [\[CrossRef\]](#)
27. Langford, J.I.; Wilson, A.J.C. Scherrer after Sixty Years: A Survey and Some New Results in the Determination of Crystallite Size. *J. Appl. Crystallogr.* **1978**, *11*, 102–113. [\[CrossRef\]](#)
28. Golubkov, V.V.; Dymshits, O.S.; Petrov, V.I.; Shashkin, A.V.; Tsenter, M.Y.; Zhilin, A.A.; Kang, U. Small-Angle X-Ray Scattering and Low-Frequency Raman Scattering Study of Liquid Phase Separation and Crystallization in Titania-Containing Glasses of the ZnO-Al<sub>2</sub>O<sub>3</sub>-SiO<sub>2</sub> System. *J. Non-Cryst. Solids* **2005**, *351*, 711–721. [\[CrossRef\]](#)
29. Alekseeva, I.; Baranov, A.; Dymshits, O.; Ermakov, V.; Golubkov, V.; Tsenter, M.; Zhilin, A. Influence of CoO Addition on Phase Separation and Crystallization of Glasses of the ZnO-Al<sub>2</sub>O<sub>3</sub>-SiO<sub>2</sub>-TiO<sub>2</sub> System. *J. Non-Cryst. Solids* **2011**, *357*, 3928–3939. [\[CrossRef\]](#)
30. Ghose, S.; Choudhury, N.; Chaplot, S.L.; Pal Chowdhury, C.; Sharma, S.K. Lattice Dynamics and Raman Spectroscopy of Protoenstatite Mg<sub>2</sub>Si<sub>2</sub>O<sub>6</sub>. *Phys. Chem. Miner.* **1994**, *20*, 469–477. [\[CrossRef\]](#)
31. Okuno, M.; Zotov, N.; Schmücker, M.; Schneider, H. Structure of SiO<sub>2</sub>-Al<sub>2</sub>O<sub>3</sub> Glasses: Combined X-Ray Diffraction, IR and Raman Studies. *J. Non-Cryst. Solids* **2005**, *351*, 1032–1038. [\[CrossRef\]](#)
32. Wang, Z.; Wang, Z.; Gan, L.; Zhang, J.; Wang, P. Structure/Property Nonlinear Variation Induced by Gamma Ray Irradiation of Boroaluminosilicate Transparent Glass Ceramic Containing Gahnite Nanocrystallite. *J. Non-Cryst. Solids* **2022**, *578*, 121346. [\[CrossRef\]](#)
33. Vasanthavel, S.; Ezhilan, M.; Ponnillavan, V.; Ferreira, J.M.F.; Kannan, S. Manganese Induced ZrSiO<sub>4</sub> Crystallization from ZrO<sub>2</sub>SiO<sub>2</sub> Binary Oxide System. *Ceram. Int.* **2019**, *45*, 11539–11548. [\[CrossRef\]](#)

34. Cormier, L. Nucleation in Glasses—New Experimental Findings and Recent Theories. *Procedia Mater. Sci.* **2014**, *7*, 60–71. [[CrossRef](#)]
35. Rice, R.W.; McMillan, P.W.; Stryjak, A.J. Internal Stress Dependence of the Hardness of Crystallized Glasses. *J. Mater. Sci.* **1979**, *14*, 2768–2772. [[CrossRef](#)]
36. Huang, J.; Zhang, J.; Yu, Y.; Bai, H.; Zhang, Z.; Huang, Y. Transparent MgO–Al<sub>2</sub>O<sub>3</sub>–SiO<sub>2</sub> Glass-Ceramics Prepared with ZrO<sub>2</sub> and SnO<sub>2</sub> as Nucleating Agents. *J. Non-Cryst. Solids* **2022**, *588*, 121585. [[CrossRef](#)]
37. Sant’Ana Gallo, L.; Célerié, F.; Bettini, J.; Rodrigues, A.C.M.; Rouxel, T.; Zanotto, E.D. Fracture Toughness and Hardness of Transparent MgO–Al<sub>2</sub>O<sub>3</sub>–SiO<sub>2</sub> Glass-Ceramics. *Ceram. Int.* **2022**, *48*, 9906–9917. [[CrossRef](#)]

**Disclaimer/Publisher’s Note:** The statements, opinions and data contained in all publications are solely those of the individual author(s) and contributor(s) and not of MDPI and/or the editor(s). MDPI and/or the editor(s) disclaim responsibility for any injury to people or property resulting from any ideas, methods, instructions or products referred to in the content.